Virtual Real Source: Source signature estimation using seismic interferometry

Jyoti Behura[1] and Roel Snieder[1]

ABSTRACT

Knowledge of the seismic source signature is crucial in numerousproblems in exploration seismology, especially in full-waveform inversion. However, existing methods of source signature estimation like statistical methods and well-log-based methods suffer from several drawbacks arising from assumptions such as whiteness of the reflectivity series and the minimum-phase character of the wavelet. Also, estimation of the source signature using wave-theoretical methods requires the recording of the wavefield and its normal derivative or additional recordings above the receiver surface which are not always available. We introduce a method, called the Virtual Real Source, of extracting the source signature based on the theory of seismic interferometry, also known as the virtual source method. This method is independent of the assumptions and drawbacks of the above-mentioned methods. The only requirement for the method of Virtual Real Source is to have a virtual source location coincide with the physical shot position whose source signature is desired. The virtual source location does not necessarily have to be a zero-offset receiver because one can use interpolation for it. The source signature is extracted by deconvolving the real recording at a receiver from the virtual source recording. Through modeling examples, we show that Virtual Real Source produces accurate source signatures even for complicated subsurface structures and source signatures, and is robust in the presence of noise. Source signature of every shot in a survey can be extracted reliably as long as the source signatures have similar amplitude spectra. The phase spectrum of the source signature is always extracted accurately even if it varies randomly from one shot to another. The Virtual Real Source applied on a 2D streamer data set from the North Viking Graben in the North Sea extracts all the airgun signatures with the main pulse and the bubble oscillation.

INTRODUCTION

Seismic source signature estimation is an important problem in reflection seismology. Amundsen (2000) notes that, "Areas where this knowledge (of source signature) is potentially of great value are on-board source array QC (quality control), deconvolution, multiple attenuation, tying reflection data to wells, modeling and inversion, AVO analysis, reservoir monitoring, and analysis of marine multicomponent recordings." For example, crosscorrelation of the source wavefield generated using an incorrect source signature with the receiver wavefield would generate an incorrect image at zero lag (even if the correct velocity model is used). Also, knowledge of the source signature is critical in full-waveform inversion (Pratt and Shipp, 1999; Ravaut et al., 2004). Moreover, other applications such as multiple prediction/suppression and auto-focusing (Rose,

2002a, 2002b; Behura et al., 2012; Broggini and Snieder, 2012; Wapenaar et al., 2013) need the correct source signature. However, it is worth noting that the surface-multiple-prediction algorithm of Verschuur and Berkhout (1997) estimates the source signature as well. Therefore, it is necessary to know the source signature accurately, which when deconvolved from the seismic data helps to correctly position reflectors and estimate reflection amplitudes.

A direct measurement of the source signature of an airgun, an airgun array, or a dynamite explosion, can be made by recording the direct far-field wave from these sources after correcting for geometrical spreading. The recorded signal, however, might be contaminated with scattered waves and also might not even be the far-field signature. In offshore acquisition, air-gun arrays are often used instead of single airguns. Dragoset (2000) points out that the disadvantage of using an array-like seismic source is that

---

measuring the output is difficult. In this case, source-detector position is crucial and the positioning should be such that it is equidistant from all the elements of the array, which is rarely the case. In land acquisition, it is normally impossible to measure the source signature of dynamite directly because of the difficult task of separating the direct wave from scattered waves (Ziolkowski, 1993).

Because of the challenges and high cost in measuring the source signature directly in the field, researchers have proposed alternative methods and algorithms to estimate the source signature. Source signature estimation based on statistical methods (Robinson and Treitel, 1980; Oldenburg et al., 1981; Hargreaves, 1992) suffer from several drawbacks. These methods assume the source signature to be of minimum-phase, the earth response to be white, and the seismic data to be stationary and noise-free (Yilmaz, 2001). These assumptions are often not met, which can make the extracted source signature unreliable. Methods based on well-logs are prone to errors as well because they require the application of a true-amplitude processing sequence that eliminates multiples, compensates for geometrical spreading and transmission losses, etc. (Buland and Omre, 2003).

Other approaches based on linear and nonlinear inversion (Landrø and Sollie, 1992; Amundsen, 1993, 2000; Landrø et al., 1994), need data to be recorded at a mini-streamer located below the source array and also assume the scattered energy recorded by the mini-streamer to be negligible.

Wave-theoretical methods of source signature extraction (Weglein and Secrest, 1990; Osen et al., 1998) are more accurate compared to the other existing methods. A significant advantage of these methods is their ability to extract source array patterns. These methods, however, assume that the medium above the recording surface is known and that the wavefield and its normal derivative are measured (Weglein and Secrest, 1990), which is the case only in OBC and dual-sensor towed streamer surveys (Tenghamn et al., 2007). To alleviate the recording of the normal derivative of the wavefield, Osen et al. (1998) propose a modification to the method of Weglein and Secrest (1990). This modification, however, introduces the requirement of additional (one or more) recordings above the receiver surface. Moreover, the algorithm of Osen et al. (1998) estimates signatures only of point sources; for an array of guns, the method requires knowledge of the locations of the individual guns in addition to mini-streamer recordings above the receiver surface.

The abovementioned drawbacks and assumptions involved in source signature estimation call for a method of source signature extraction with a bare minimum of assumptions and requirements. Here, we introduce a novel method, named Virtual Real Source (Behura, 2007), for determination of the seismic source signature based on the principle of seismic interferometry. Through synthetic data examples, we show that this method produces accurate source signatures even for complicated subsurface structures and source signatures. We also present a field data example where Virtual Real Source does a satisfactory job at extracting the airgun signatures.

A SIMPLE IDEA

In seismic interferometry, the acoustic Green's function between any two receiver locations can be computed by crosscorrelating the receiver recordings due to random sources (Lobkis and Weaver, 2001; Derode et al., 2003a, 2003b; Snieder, 2004; Wapenaar et al., 2004; Weaver and Lobkis, 2004; Curtis et al., 2006) or transient sources (Snieder et al., 2006; Wapenaar and Fokkema, 2006)

$$U_{virt}(\mathbf{x}_B, \mathbf{x}_A, \omega)$$
$$= n \oint_{\partial \mathbb{D}} |S(\mathbf{x}, \omega)|^2 G(\mathbf{x}_A, \mathbf{x}, \omega) G^*(\mathbf{x}_B, \mathbf{x}, \omega) d^2\mathbf{x} + se, \quad (1)$$

where ω represents the frequency, U_{virt} is the scaled impulse response obtained by crosscorrelation of wavefields recorded at $\mathbf{x}_A$ and $\mathbf{x}_B$, n denotes the number of sources per unit surface area, G is the Green's function, $|S(\mathbf{x}, \omega)|$ is amplitude spectrum of the shot at $\mathbf{x}$, "se" denotes the spurious events, and "$*$" denotes the complex conjugate. Similar equations for elastic media can be found in Wapenaar and Fokkema (2006). Equation 1 is a surface integral over sources distributed on $\partial \mathbb{D}$. Note that U_{virt} contains the superposition of the causal and anticausal parts of the Green's function between $\mathbf{x}_A$ and $\mathbf{x}_B$. If the amplitude spectra of all the source signatures inside the integral in equation 1 are the same, then equation 1 becomes

$$U_{virt}(\mathbf{x}_B, \mathbf{x}_A, \omega)$$
$$= n|S(\omega)|^2 \oint_{\partial \mathbb{D}} G(\mathbf{x}_A, \mathbf{x}, \omega) G^*(\mathbf{x}_B, \mathbf{x}, \omega) d^2\mathbf{x} + se, \quad (2)$$

where $S(\omega)$ is the source signature.

The spurious events are introduced in the reconstructed Green's function because of a high-frequency approximation made in deriving equation 1. These events can be suppressed by assuming the medium outside $\partial \mathbb{D}$ to be homogeneous. Equation 1 is strictly valid for a closed source aperture, i.e., the true Green's function between the two receivers can be obtained if there are sources on a closed surface surrounding the two receivers. In reality, for a seismic survey, the receivers are usually not surrounded by sources on all sides. This incomplete source aperture can result in other spurious events which could possibly be suppressed through tapering the correlograms. Equation 1 is only valid if the medium is nonattenuative. In reality, however, the subsurface is always attenuative which incorporates certain error into the reconstructed Green's function. Derivation of equation 1 also assumes the use of only monopole-source recordings which, in combination with the parameter n, introduces an amplitude-scaling error without affecting the phase. In elastic media, however, one requires monopole and dipole P- and S-wave sources to accurately reconstruct U_{virt}. Because only monopole sources are available in most seismic surveys (as well as in the modeling examples here), the reconstructed U_{virt} could have some spurious events and an amplitude-scaling error but no phase error (Wapenaar and Fokkema, 2006). The spurious events would introduce some error into the estimated source signature, but the amplitude error would have no influence because it is only a scaling factor.

Following equation 1, to determine the Green's function between any two receiver locations (e.g., A and B in Figure 1a), the recordings at these two locations are cross-correlated for every source. The crosscorrelations are summed over all the shots to obtain the Green's function between the two receiver locations. This principle has been applied to exploration seismology to remove overburden problems (Calvert et al., 2004; Bakulin and Calvert, 2006) and in imaging the subsurface (Schuster et al., 2004).

The crosscorrelation operation in equation 2, however, does not yield the true Green's function; instead it gives the scaled impulse response $U_{virt}(\mathbf{x}_B, \mathbf{x}_A, \omega)$:

$$U_{virt}(\mathbf{x}_B, \mathbf{x}_A, \omega) = n|S(\omega)|^2 G(\mathbf{x}_B, \mathbf{x}_A, \omega). \qquad (3)$$

For simplicity, the term corresponding to the spurious events in equation 3 has been omitted. In equation 3, the amplitude spectrum of all the sources used in computing $U_{virt}(\mathbf{x}_B, \mathbf{x}_A, \omega)$ is assumed to be the same ($|S(\mathbf{x}, \omega)| = |S(\omega)|$); later, we discuss the case where this assumption is not valid. Note that the wavefield $U_{virt}(\mathbf{x}_B, \mathbf{x}_A, \omega)$ is independent of the phase spectrum of the source signature.

If the virtual source location A coincides with an actual shot location, then at receiver B there is an active recording due to the actual shot at A (Figure 1b)

$$U_{real}(\mathbf{x}_B, \mathbf{x}_A, \omega) = S(\omega) G(\mathbf{x}_B, \mathbf{x}_A, \omega). \qquad (4)$$

Here, the word "*real*" implies "*actual*" (as opposed to the real part of a complex number).

From equations 3 and 4, it follows that deconvolving the scaled impulse response (equation 3) from the active recording (equation 4) and taking its complex conjugate yields the true source signature. In practice, we perform this operation in the frequency domain by dividing the spectra of the two recordings:

$$\left[\frac{U_{virt}(\mathbf{x}_B, \mathbf{x}_A, \omega)}{U_{real}(\mathbf{x}_B, \mathbf{x}_A, \omega)}\right]^* = nS(\omega). \qquad (5)$$

To stabilize the deconvolution in equation 5, we use the following estimator for the deconvolution instead

$$\left[\frac{U_{virt}(\mathbf{x}_B, \mathbf{x}_A, \omega) U_{real}^*(\mathbf{x}_B, \mathbf{x}_A, \omega)}{|U_{real}(\mathbf{x}_B, \mathbf{x}_A, \omega)|^2 + \epsilon}\right]^* = nS(\omega), \qquad (6)$$

where the parameter ϵ is set to 0.1% of the average spectral power in this study. Note from equation 6 that the extracted source signature is a scaled version (by a factor of n) of the true source signature.

Because the scaled impulse response, aka *virtual* source record, is deconvolved with the *real* active recording to obtain the *source* signature, this method is named "Virtual Real Source." Note that the only requirement for this method is to have a receiver at the location previously occupied by the shot (the shot whose source signature we are interested in), and *not necessarily* at a zero-offset receiver. Apart from this requirement and the error introduced by the imperfect scaled impulse response, there are no assumptions for this method to work; we do not need any prior information about the subsurface. If this requirement is not met, one could perform interpolation of traces to obtain an acquisition geometry suitable for source extraction using Virtual Real Source; an example of Virtual Real Source applied on interpolated receivers is shown later.

Figure 2 illustrates a scenario where a virtual source coincides with a real source. For a real (physical) shot at A, one has an active recording at B [$U_{real}(\mathbf{x}_B, \mathbf{x}_A, \omega)$]. As more shots are fired by moving the whole source-receiver array, one has a 2D seismic survey. Using these 2D data, the virtual source function $U_{virt}(\mathbf{x}_B, \mathbf{x}_A, \omega)$ between the points A and B (with A_{vs} as the virtual source) is computed by equation 3. Substituting $U_{virt}(\mathbf{x}_B, \mathbf{x}_A, \omega)$ and $U_{real}(\mathbf{x}_B, \mathbf{x}_A, \omega)$ into equation 6, one can compute the source signature of the shot at A. Note again that, in this survey, we do not have and do not need any zero-offset recording for computing the source signature. The coincidence of the virtual source location with the real source also means that their vertical depths be the same.

This is true for most land- and streamer-acquisitions where the difference in the depths of the sources and receivers is within a fraction of the wavelength. For OBC surveys, the source wavefield has to be downward continued to the receiver level before the application of Virtual Real Source.

SYNTHETIC DATA TESTS

Figure 3 shows a layer-cake model used for testing the idea described in the previous section. The shots are on the surface at an equal spacing of 25 m spanning a total length of 5 km. The receivers lie on the surface to the right of each shot and also spread for 5 km at
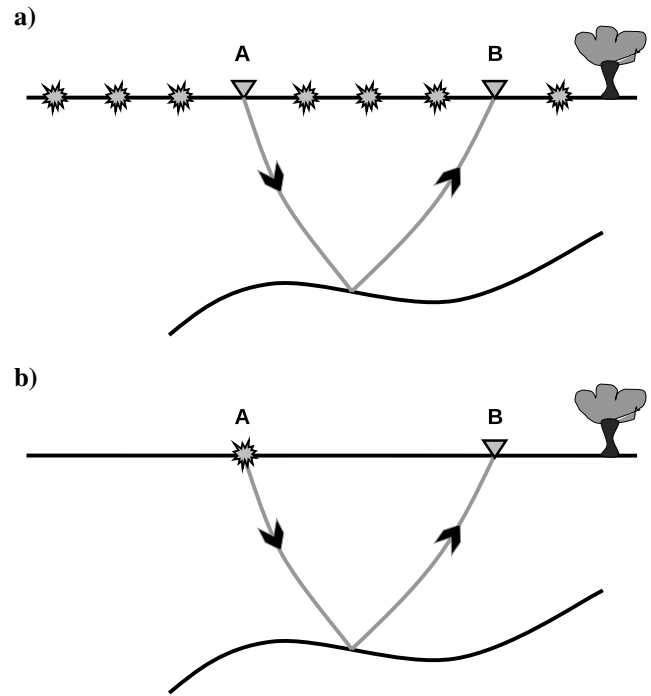
a)

b)

Figure 1. Illustration for the computation of the (a) scaled impulse response U_{virt} and (b) the real recording U_{real} between two receiver locations A and B. The stars represent shots and the triangles represent receivers.
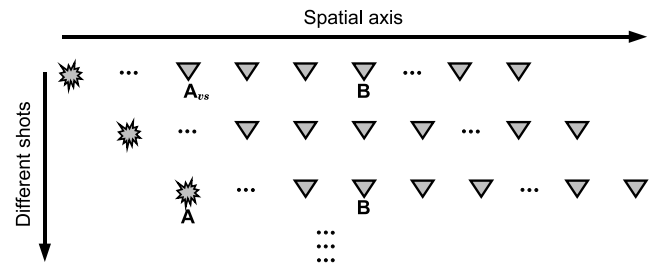

Figure 2. Illustration of a routine 2D seismic survey. The different source-receiver lines represent consecutive shot-lines achieved by moving the whole source-receiver array along a 2D line. Other 2D surveys shown later are illustrated in a similar fashion. The location of the physical source A coincides with that of the virtual source A_{vs}. As in Figure 1, stars represent shots and triangles represent receivers.

25 m intervals. A 30 Hz dominant frequency Morlet wavelet (real part) is used as the source signature. We model the SH-wave for this example and for all the examples that are to follow unless otherwise mentioned. The theory, however, is valid for all components of excitation and recording because the scaled impulse response can be generated for all components (Draganov et al., 2006; Wapenaar and Fokkema, 2006).

To obtain the correct amplitude and phase, the impulse response $U_{virt}(\mathbf{x}_B, \mathbf{x}_A, \omega)$ has to be scaled by $-i\omega$ for sources spread on the surface and by $\sqrt{-i\omega}$ for source distribution along a line (Snieder
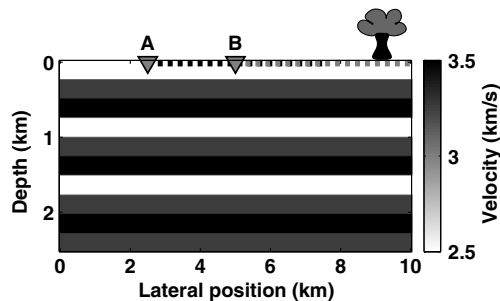
Figure 3. The SH-wave velocity model and the acquisition used for testing Virtual Real Source. The top boundary is a free-surface and the rest are absorbing boundaries. The two receiver locations A and B are marked by triangles. The source spread for receiver A is denoted by the dashed black line and that for receiver B by the dashed gray line. Sources are uniformly spaced at 25 m interval.
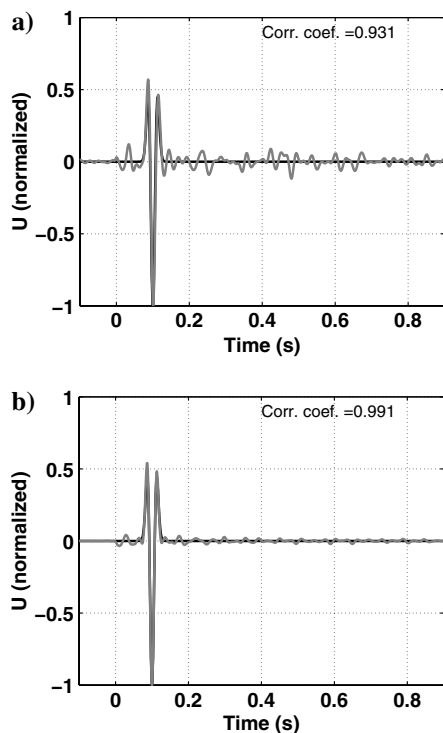
Figure 4. (a) The actual (black line) and the extracted (gray line) source signatures for only one source-receiver combination and (b) the source signature obtained after averaging over 201 source-receiver combinations. The zero-lag crosscorrelation coefficient between the extracted and the actual source signatures is also given to quantify the accuracy of source extraction.

et al., 2006). Because all the examples shown here are in 2D, the impulse response is scaled by $\sqrt{-i\omega}$. The major difference between $U_{real}(\mathbf{x}_B, \mathbf{x}_A, t)$ and $U_{virt}(\mathbf{x}_B, \mathbf{x}_A, t)$ comes from the influence of the source signature. It is, however, important to note that the scaled impulse response is not perfect because of the assumptions involved in its derivation (Wapenaar and Fokkema, 2006). Violation of these assumptions introduces spurious events (Snieder et al., 2006) in the reconstructed impulse response (equation 1) which in turn manifest in some inaccuracy in the extracted source signature as shown below.

The signature extracted using Virtual Real Source for the above numerical experiment is given in Figure 4a after normalization. The actual source signature used in modeling is also shown for comparison (also normalized). To quantify the accuracy of the source signature estimation, the zero-lag cross-correlation coefficient between the two is also given. The signature is well-recovered as can be seen from the good match in the waveform and initiation time with a zero-lag cross-correlation coefficient of 0.931. However, there are some spurious events resulting from the imperfect virtual source function.

The source signature in Figure 4a is extracted (using equation 6) for only one source-receiver combination. By choosing a different location of B in Figure 3, another estimate of the source signature for shot A can be extracted. Thus, independent estimates of the source signature of shot A can be extracted for different locations of receiver B. Averaging these independently extracted source signatures improves the accuracy of estimation substantially as evident from Figure 4b. Instead of a simple average of the various estimates of the source signature of shot A, one could alternatively solve equation 5 for $S(\omega)$ simultaneously for all locations of receiver B using weighted least-squares inversion (Aster et al., 2012).

Because there are no limitations on the amplitude and phase of the source signature, any source signature can be extracted accurately using Virtual Real Source. Figure 5 shows a source signature that would be considered complicated relative to the source signatures used in routine seismic processing. Even for such a source signature with complicated phase and amplitude spectra, Virtual Real Source is able to extract it with acceptable accuracy.

Also, because there are no assumptions on the heterogeneity of the subsurface in source signature extraction using Virtual Real Source, it works well for any arbitrarily complicated subsurface. This can be seen for the Sigsbee model in Figure 6a. The acquisition involves sources at a depth of 4 m at equal intervals of 45.72 m (Figure 6b). The receivers are also located at 4 m depth to the right of each shot, spread over 2644.1 m at equal intervals of 22.86 m. For this acquisition geometry, the maximum number of sources summed over in computing the scaled impulse response between any two receiver locations is 174. The source signature (stacked over 348 estimates) extracted for the shot at 14.714 km is shown in Figure 7. From the above examples, it is clear that Virtual Real Source is able to extract even complicated source signatures accurately from data acquired over complicated subsurface geometries.

Virtual Real Source in elastic media

Interferometry in elastic media is more involved in comparison to acoustic media (Wapenaar and Fokkema, 2006). Reconstruction of the scaled impulse response in elastic media requires recordings from P- and S-wave sources with different polarizations. For example, to obtain the zz-component (vertical components of

source and receiver) of the scaled impulse response, we need to sum the zz-impulse responses obtained from all sources of excitation, namely x-, y-, z-, and p-excitations (p denotes a pressure source). In most seismic surveys, however, not all of these sources of excitation exist — on land, the source is mostly a vertical force or a P-wave source (dynamite), whereas in offshore acquisition the source is almost always a pressure source.

Therefore, in the next example, we use only the vertical components of excitation and recording to compute the zz-component of the scaled impulse response. The horizontal components of the sources have not been used in reconstructing $U_{virt,zz}$ because the energy in the vertical components of receivers from these sources is small. Hence, $U_{virt,zz}$ is reconstructed with sufficient accuracy even if only the vertical components of sources are used. This results in high accuracy of the extracted source signature (Figure 8).

SOURCE VARIABILITY

Source signature estimation using Virtual Real Source works well if all the sources are the same (equation 2), i.e., they have the same source signature. But this is not usually the case in the field where source signatures can vary widely. What happens if the source signatures vary within the survey? A closer inspection of the Virtual Real Source process reveals that source variability does not pose a major problem. This is because after cross-correlation and summation, the source signature in the virtual source function, denoted by S_{avg}, is a weighted-average over all source signatures used in computing U_{virt} (Snieder et al., 2007); in this case, equation 1 becomes
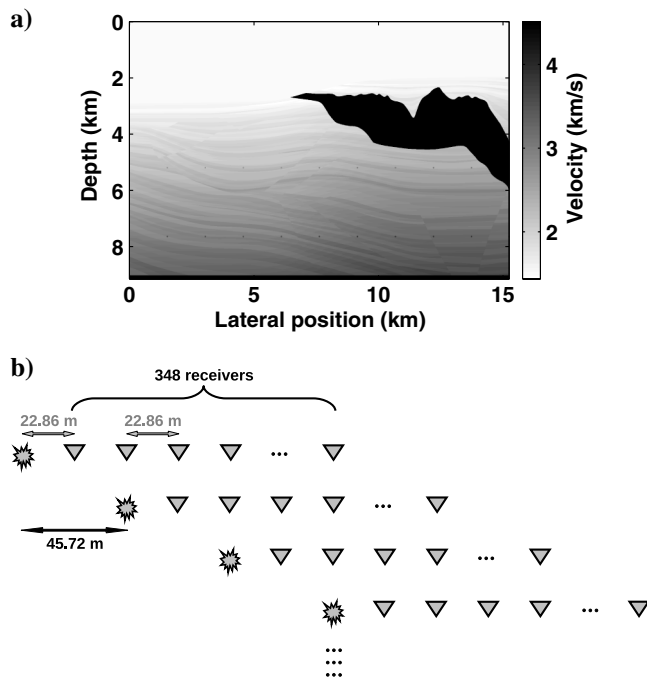

Figure 6. (a) The Sigsbee P-wave velocity model and (b) the 2D data-acquisition design. The different source-receiver lines represent consecutive shot-lines achieved by moving the whole source-receiver array along a 2D line. In total, 500 shots are fired and the wavefield is recorded at 348 receivers for each shot.

Figure 5. The actual (black line) and the extracted (gray line) signature (a) for a complicated source signature and the corresponding amplitude (b) and phase (c) spectra. The model and acquisition geometry are shown in Figure 3. The mismatch in the phase spectrum is present only for frequencies with insignificant amplitudes.
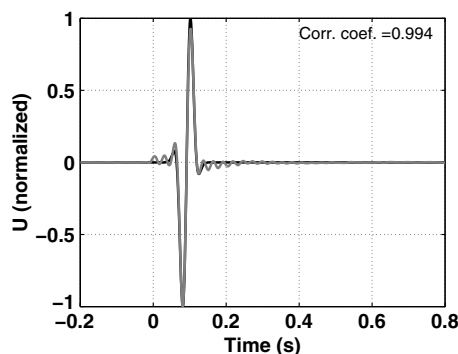

Figure 7. The actual (black line) and the extracted (gray line) source signatures at location $x = 14.714$ km for the Sigsbee model in Figure 6a. The extracted source signature has been stacked over 348 estimates of the source signature.

$$U_{virt}(\mathbf{x}_B, \mathbf{x}_A, \omega) = n|S_{avg}(\omega)|^2 G(\mathbf{x}_B, \mathbf{x}_A, \omega). \qquad (7)$$

The weights in the weighted-average $S_{avg}(\omega)$ are determined by the stationary phase contributions of the sources; the maximum contribution comes from the stationary points on $\partial\mathbb{D}$ (Snieder et al., 2006). In the presence of source-signature directivity (e.g., source signature of air-gun array), $S_{avg}(\omega)$ will comprise additional weighted-averaging (again determined by the stationary phase contributions) over direction. Also, under such circumstances, equation 4 will contain directionally-dependent contributions because of the directivity of $S(\omega)$; here again, $S(\omega)$ will be weighted according to the stationary phase contributions.

Substituting equations 4 and 7 into equation 5 and taking only the magnitude, we get

$$|S_{ext}(\omega)| = \frac{n|S_{avg}(\omega)|^2}{|S(\omega)|}, \qquad (8)$$

where S_{ext} represents the extracted source signature. According to equation 8, the amplitude spectrum of the source signature is extracted accurately if it is close to $|S_{avg}(\omega)|$. However, there is rarely a significant difference in amplitude spectra of sources in any seismic survey. If at all different, the amplitude spectra usually differ by a scaling factor which simply adds a scalar k to the integral in equation 2. Therefore,

$$|S_{avg}(\omega)| \asymp k|S(\omega)|. \qquad (9)$$

Similarly, taking only the phase in equation 5 yields

$$phase[S_{ext}(\omega)] = phase[S(\omega)]. \qquad (10)$$

The phase of the extracted source signature is always recovered accurately because U_{virt} does not contain any phase information of $S(\omega)$ (equation 10); all the phase-contribution in the estimate of $S(\omega)$ comes from U_{real}.

From equations 9 and 10, it is clear that even if there is a variability in source signatures, $S(\omega)$ can be estimated accurately. Though there might be some error in the amplitude spectrum of the extracted source signature, the phase spectrum is always extracted accurately. The numerical examples below corroborate the conclusions drawn above.
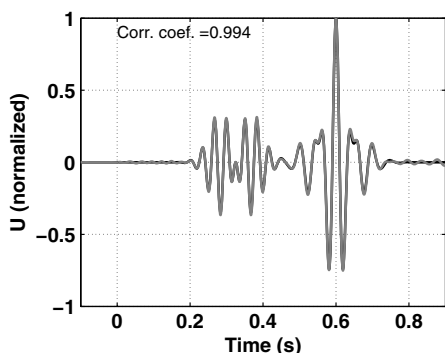
Figure 8. The actual (black line) and the extracted (gray line) source signatures using the vertical component of PSV data. The model and acquisition geometry are shown in Figure 3.

Random variation in phase spectra

The model and acquisition geometry used for this test are shown in Figure 9. In the first test, the source signature changes phase randomly (between 0 and 2π) from one shot to the next, with the amplitude spectrum remaining the same. A receiver gather from this survey is shown in Figure 10. Note that, although the continuity in reflections is evident, there is a change in phase.

The source signature extracted for the shot at location 5575 m is shown in Figure 11. The zero-lag correlation coefficient of the cross-correlation between the extracted and the actual source signatures is 0.972. Note the accuracy of the extracted phase spectrum shown in Figure 11c. All the source signatures in the survey are extracted with high accuracy as evident from the high correlation coefficients in Figure 12. This test confirms the earlier conclusion that even for a complicated change in phase spectrum of the sources in the survey, the source signatures can be extracted reliably as long as they all have similar amplitude spectra.

Influence of amplitude spectra

The above example can be complicated further by randomly varying the amplitude spectra as well. The amplitude spectrum
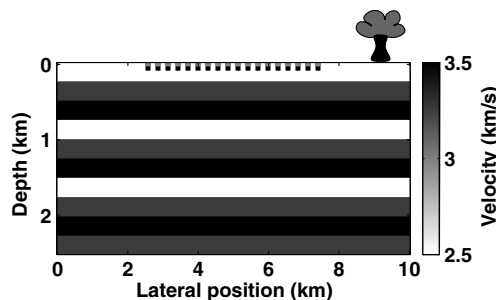
Figure 9. The acquisition used in the numerical examples in the random-phase-spectra and random-amplitude-and-phase-spectra tests. Sources and receivers are spread on the surface along the black and gray dashed lines, respectively, at equal intervals of 25 m.
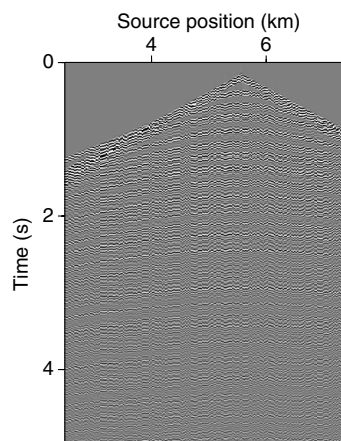
Figure 10. Receiver gather at location $x = 5575$ m for the random-phase-spectra test. The sources have different phase spectra but the same amplitude spectrum. Although the record spans over 10 seconds, only the first five seconds of the data are shown for clarity.
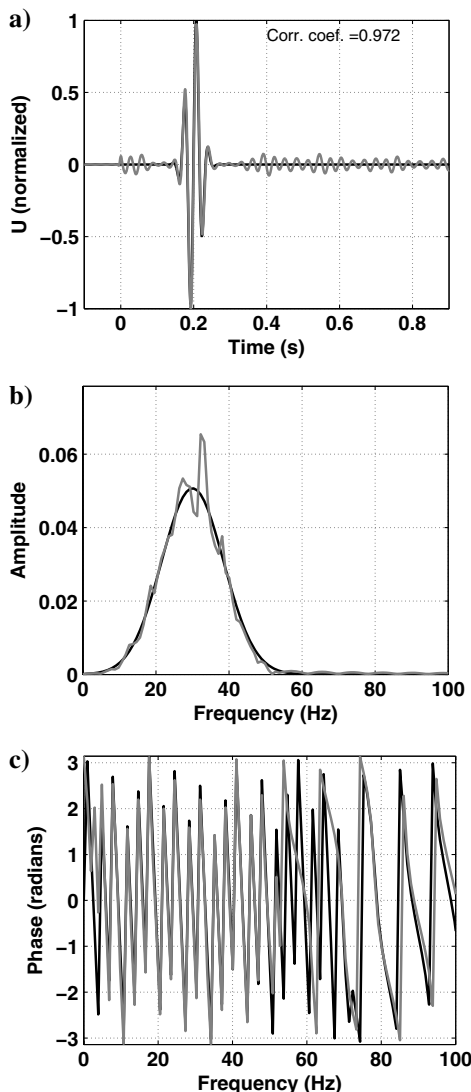
Figure 11. The actual (black line) and the extracted (gray line) source signatures (a) and the corresponding amplitude (b) and phase (c) spectra for the shot at location $x = 5575$ m in the random-phase-spectra test.
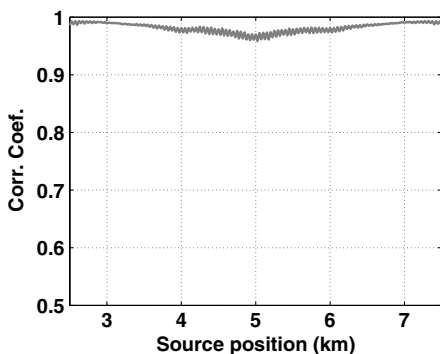

Figure 12. The zero-lag crosscorrelation coefficients between the extracted source signatures with the actual signatures for the random-phase-spectra test.

is varied by randomly changing the dominant frequency (between 30 Hz and 40 Hz), the signal length, and the peak amplitude (between a factor of one and five) of the Morlet wavelets. A receiver gather (at $x = 5575$ m) for this test is shown in Figure 13. Unlike in Figure 10, no continuity of reflections is visible in Figure 13 because of the random change in the amplitude spectrum. Even for this case, the source signatures are extracted accurately, as seen in Figures 14 and 15. The primary source of error in the extracted source signature is the incorrect estimation of the amplitude spectrum (Figure 14b), whereas the phase spectrum is extracted accurately (Figure 14c). The source signatures having amplitude spectra close to the weighted-average $|S_{avg}(\omega)|$ are extracted with better accuracy than others.

INFLUENCE OF NOISE

The reliability of any source estimation algorithm depends heavily on its robustness in the presence of noise. As mentioned earlier, well-log-based and statistical source-estimation algorithms assume noise-free data. But, because field data always has some degree of noise, we test the performance of Virtual Real Source on a synthetic data set contaminated with noise. Here, we define noise as waves emanating from a source (different from the active sources) at some spatial location; any waves originating from the shot location are part of the source signature. Such an acquisition is shown in Figure 16 where the noise source N contaminates the shot gather for the shot at A. The noise source signature (Figure 17a) has the same amplitude spectrum as the actual source on the surface but their phase spectra differ by $\pi/4$. No other shot gathers are influenced by the noise source.

The recording at A is given by

$$U_{real}(\omega) = S_A(\omega)G(\mathbf{x}_B, \mathbf{x}_A, \omega) + S_N(\omega)G(\mathbf{x}_B, \mathbf{x}_N, \omega),$$
(11)

where $S_A(\omega)$ and $S_N(\omega)$ are the source signatures of shot A and noise-source N, respectively. The extracted source signature $S_{A,ext}(\omega)$ at A using equation 5 is given by
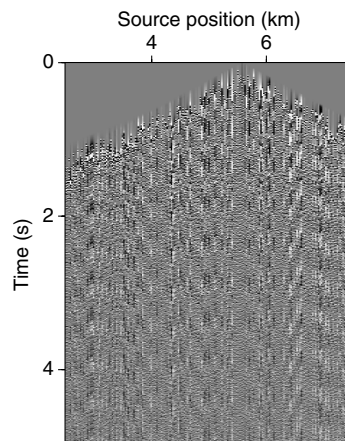

Figure 13. (a) Receiver gather at location $x = 5575$ m for the random-amplitude-and-phase-spectra test. The sources differ in amplitude and phase spectra. Although the record spans over 10 seconds, only the first five seconds of the data are shown for clarity.
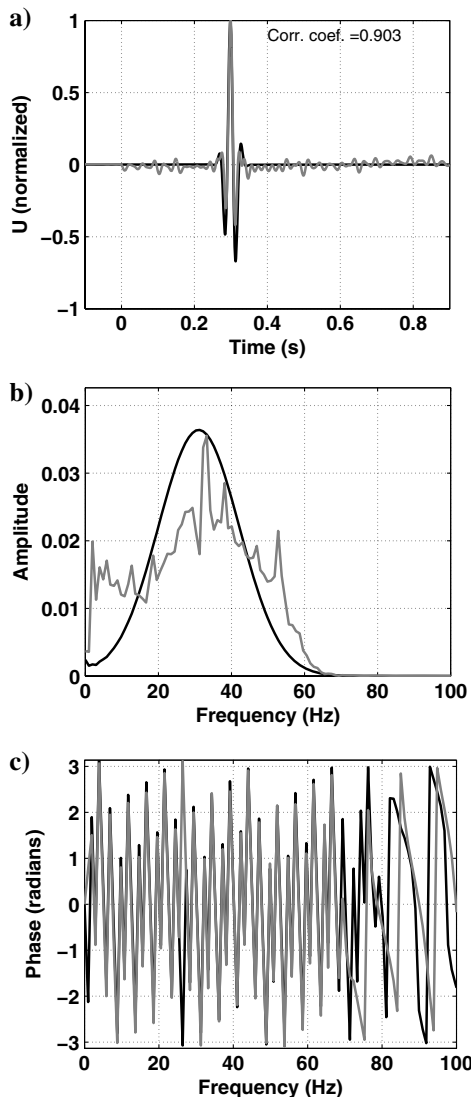
a)

b)

c)

Figure 14. The actual (black line) and the extracted (gray line) source signatures (a) and the corresponding amplitude (b) and phase (c) spectra for the shot at location $x = 5575$ m in the random-amplitude-and-phase-spectra test.
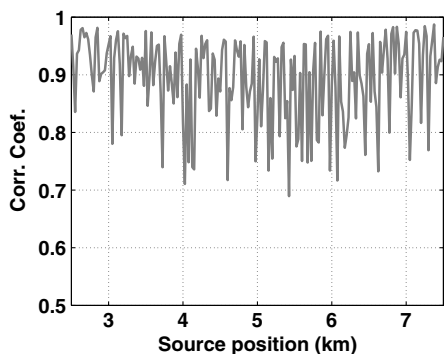

Figure 15. The zero-lag crosscorrelation coefficients of the extracted source signatures with the actual signatures for the random-amplitude-and-phase-spectra test.

$$S_{A,ext}(\omega) = \left[\frac{|S_A(\omega)|^2 G(\mathbf{x}_B, \mathbf{x}_A, \omega)}{S_A(\omega) G(\mathbf{x}_B, \mathbf{x}_A, \omega) + S_N(\omega) G(\mathbf{x}_B, \mathbf{x}_N, \omega)}\right]^*$$

$$= \left[\frac{1}{1 + \epsilon_N}\right]^* S_A(\omega), \qquad (12)$$

where

$$\epsilon_N = \frac{S_N(\omega)}{S_A(\omega)} \frac{G(\mathbf{x}_B, \mathbf{x}_N, \omega)}{G(\mathbf{x}_B, \mathbf{x}_A, \omega)}. \qquad (13)$$

Because $G(\mathbf{x}_B, \mathbf{x}_A, \omega) \neq G(\mathbf{x}_B, \mathbf{x}_N, \omega)$, the quantity ϵ_N in equation 12 acts only as a deconvolution-stabilizing-factor similar to
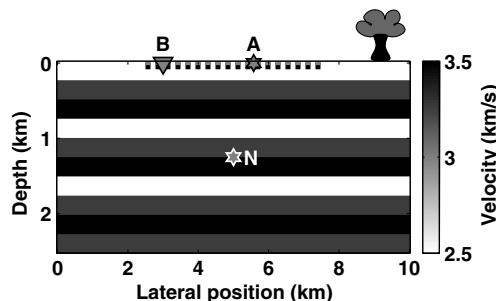
Figure 16. The acquisition geometry (same as in Figure 9) used to study the performance of Virtual Real Source in the presence of noise. The noise source N (white star) is located in the subsurface at location $x = 5000$ m and $z = 1250$ m. The shot location A, corresponding to the shot gather contaminated by the noise source N, is marked by the black star ($x = 5575$ m on the surface).
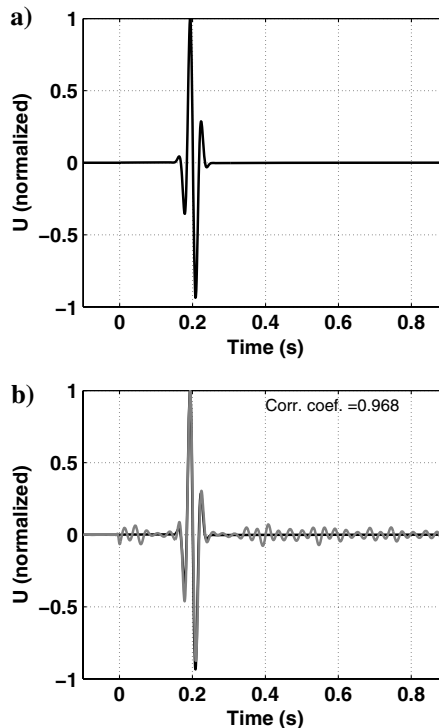
a)

b)

Figure 17. (a) The source signature of the noise source N in Figure 16. (b) The actual (black line) and the extracted (gray line) source signatures for the shot at location $x = 5575$ m.

the parameter ϵ in equation 6. Note that equation 12 resembles Wiener filtering with the parameter ϵ_N serving as the noise-to-signal power ratio (Gonzalez et al., 2003). It follows from equation 12 that the source signature of the shot A, whose shot gather is contaminated by noise, is extracted accurately (Figure 17b) if ϵ_N is frequency-independent. Even if the noise phase spectrum is a random series (Figure 18a), the source signature extraction is satisfactory (Figure 18b). In fact, if we could compute the virtual source function between the noise location N and any other receiver on the surface (e.g., B) $U_{NB,virt}$, then it is possible to extract even the noise source signature using equation 5. Only if the noise source location N coincides with the actual shot location A [$G(\mathbf{x}_B, \mathbf{x}_A, \omega) = G(\mathbf{x}_B, \mathbf{x}_N, \omega)$], the actual source signature would not be recovered accurately unless $S_N(\omega) = S_A(\omega)$. It is, however, highly unlikely that the origin of the noise coincides with the shot location, which makes source signature extraction using Virtual Real Source in the presence of noise quite robust. For example, cultural noise generated at some location near the survey area would not affect the source signature estimation of any shot in the survey because the noise location does not coincide with any real (active) shot location.

Random ambient noise can be considered as waves emanating from noise sources randomly distributed in the subsurface. In this case, equation 11 will have additional terms corresponding to all these noise sources. In spite of this complication, the form of equation 12 remains the same where all the noise sources will collectively act as a deconvolution stabilizing factor. It also follows from equation 8 that, in the presence of ambient noise, the true source signature would be extracted accurately as long as the amplitude spectrum of the noise does not deviate substantially from the amplitude spectra of the active sources; the phase spectrum of the source signature is always estimated accurately. If the noise amplitude spectrum is substantially different from that of the active sources, the stabilizing factor ϵ_N would become a function of frequency and thus incorporate errors into $S_{A,ext}(\omega)$.

VIKING GRABEN DATA

As a last step, we apply Virtual Real Source on a field data set to extract the source (air gun) signature. The 2D streamer data comes from the North Viking Graben in the North Sea (Keys and Foster, 1998). The seismic line consists of 1001 shot records oriented in a structural dip direction. Each shot record was recorded on 120 channels for six seconds at a sampling interval of 4 ms. The average cable depth is 10 m and the airgun array depth is 6 m.

The shot point as well as the receiver interval is 25 m, with the original acquisition geometry shown in Figure 19a. Note that, with the original geometry, any shot location A does not coincide with any other receiver location and therefore the source signature of any of the airguns cannot be computed accurately. To be able to extract source signatures using Virtual Real Source, one has to convert the acquisition geometry in Figure 19a to one as in Figure 2. To achieve this, we interpolate shot gathers to obtain an acquisition geometry as shown in Figure 19b, with a new minimum source-receiver offset of 275 m (a multiple of 25 m) instead of the original 262 m. In this modified acquisition geometry, any shot location A now coincides with a virtual source location A_{vs} which makes it possible to extract source signatures of the airguns using Virtual Real Source.

The (normalized) extracted source signatures of all the air guns in the survey are shown in Figure 20. Source signatures of the air guns

on the right edge of the survey (in the vicinity of 27 km) are not extracted accurately because of the low fold (<10). It is interesting that the weak bubble oscillation can also be seen at 0.35–0.5 s in Figure 20. No surface or receiver ghost contaminates the extracted source signature because the ghost is a part of the medium response (which is a part of the impulse response). The ghost is reconstructed by crosscorrelation of the waves reflected from the subsurface with the upgoing waves at the source; both these waves propagate outward from the sources on $\partial\mathbb{D}$ and therefore are able to reconstruct the ghost (Wapenaar and Fokkema, 2006). The difference in depths of the air gun sources and hydrophones (4 m in this case study), however, is likely to introduce minor errors in the reconstructed impulse response which in turn leaks into the extracted source signature. For more accurate signatures, receiver wavefields could be recomputed at the source depth. Conventional source signature extraction would not be able to extract such detailed source signatures. Because air gun signatures are strongly directional, it is advisable to estimate the directionality of the extracted signature in Figure 20. The minimum offset between the virtual source and any receiver is 275 m and the maximum offset is about 3000 m. Because most of the energy comes from seafloor (mean depth of 300 m) and near-seafloor reflections and because we average the source signature over all offsets, the extracted source signature should be closer to the 40° signature (from simple geometry considerations).

ADDITIONAL APPLICATIONS

Beside the obvious applications in exploration seismology, it might be possible to use Virtual Real Source in crustal seismology
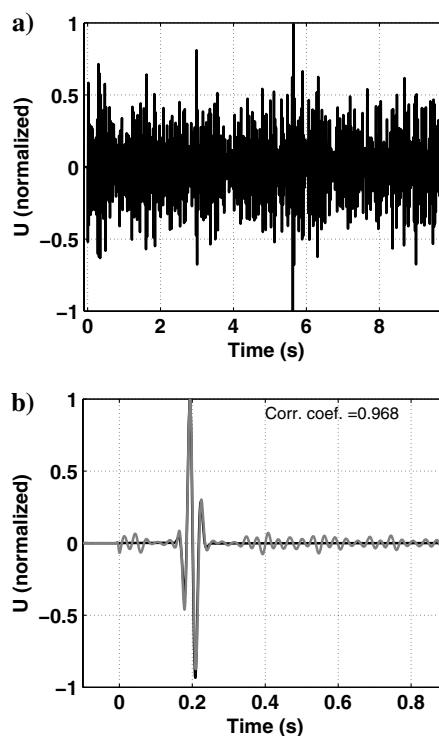
Figure 18. (a) The source signature (with a random phase spectrum) of the noise source N in Figure 16. (b) The actual (black line) and the extracted (gray line) source signatures for the shot at location $x = 5575$ m.

Figure 19. The original (a) and the modified (b) acquisition geometries for the Viking Graben data. The figures are not shown to scale. The stars represent shots and the triangles receivers. The different source-receiver lines represent consecutive shot-lines achieved by moving the whole source-receiver array along a 2D line. Note that the receiver positions change from (a) to (b); the minimum offset in (a) is 262 m whereas, for the interpolated receivers in (b), the minimum offset is 275 m. The source of interest is denoted by A whereas A_{vs} is the virtual source. In the original survey, no virtual source location coincides with A whereas in the modified survey, the interpolated receiver A_{vs} serves as the coincident virtual source.
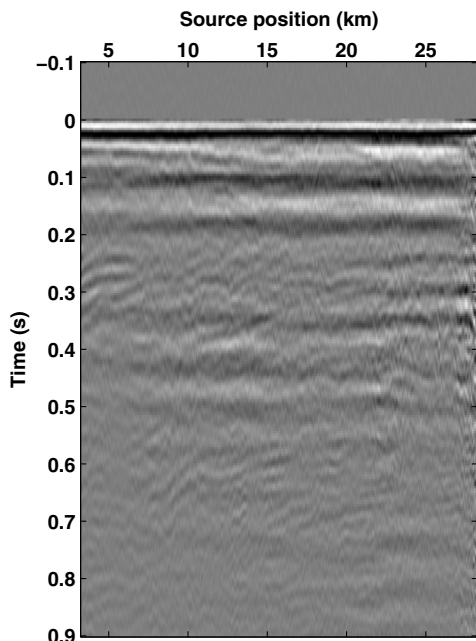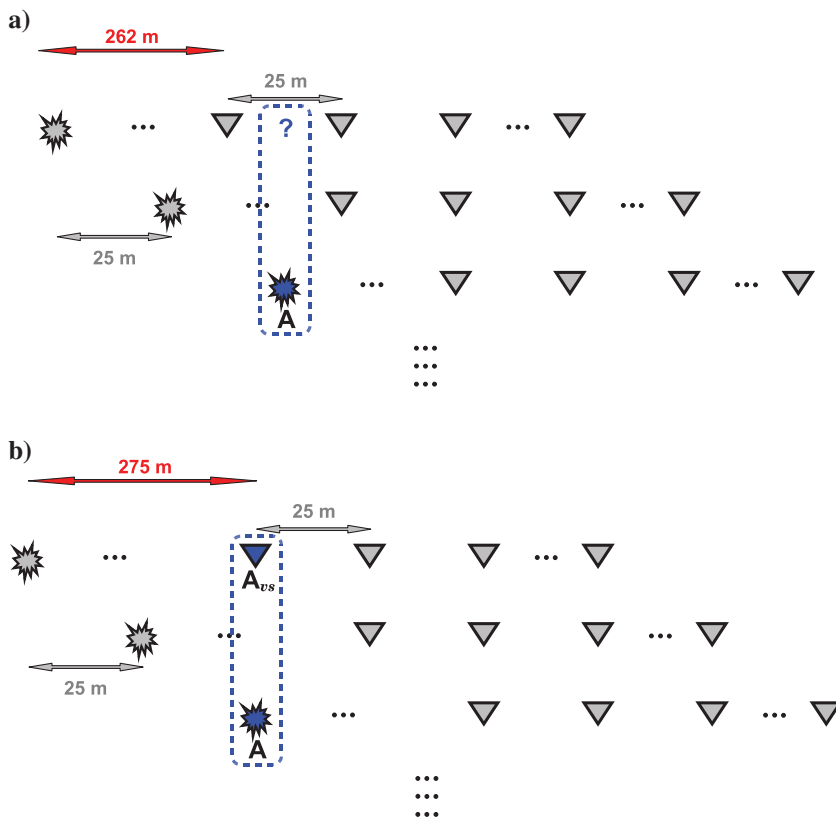
Figure 20. The source signatures (normalized) of all the airguns in the Viking Graben data extracted using Virtual Real Source. The main pulse can be seen at 0–0.2 s whereas the bubble oscillation arrives at ≈0.35 s.

to extract the source signatures of earthquakes. A shallow earthquake underneath a seismometer station recorded at some other seismometer serves as the active recording U_{real}. The virtual source function U_{virt} between these two seismometer stations can be computed using many earthquake records or ambient seismic noise (Campillo and Paul, 2003; Shapiro et al., 2005). Using U_{real} and U_{virt} in equation 5 yields the earthquake source signature.

The San Andreas Fault Observatory at Depth (SAFOD) offers an ideal opportunity to perform the above experiment. The SAFOD pilot hole is located adjacent to the San Andreas fault and houses permanent receivers that continuously record seismic activity. Cross correlation of various earthquake responses at any downhole receiver with any other remotely located seismometer yields U_{virt}. A seismic event originating in the fault zone and recorded by the remote seismometer can serve as U_{real}. With the downhole receiver serving as the virtual source, we could estimate the signature of the earthquake in the fault zone.

CONCLUSION

Apart from the limited source aperture, there are no assumptions involved in source signature extraction using the Virtual Real Source method. It is, however, important to keep in mind that the quality of the extracted source signature depends on the quality of the virtual source function. Extraction of the exact source signature necessitates the computation of the correct virtual source function, which is not always possible. However, in seismic surveys having an adequate coverage of sources and receivers, an accurate virtual source function is computed which helps in extracting a fairly accurate source signature.

Virtual Real Source is valid for all components of excitation and recording and no prior information about the subsurface is needed. The only requirement for the method, however, is that the physical source location must coincide with a virtual source location. This *does not* mean that one needs a zero-offset receiver, but rather one needs a receiver location to lie at the shot location whose source signature is desired. In the case where an actual receiver location does not coincide with the shot location, an interpolated receiver can be used as the virtual source. Virtual Real Source can extract source signatures accurately even if the phase spectra of the source signatures are completely different, as long as their amplitude spectra are similar. Because of the lack of any assumptions, Virtual Real Source works well for complicated subsurface geometries and complicated source signatures.

ACKNOWLEDGMENTS

REFERENCES

Ampuero, J.-P., 2002, Etude physique et numérique de la nucléation des séismes: Ph.D. thesis, Université Paris.
Amundsen, L., 1993, Estimation of source array signatures: Geophysics, **58**, 1865–1869, doi: 10.1190/1.1443402.
Amundsen, L., 2000, Linear inversion for source signatures from mini streamer data: The Leading Edge, **19**, 40–43, doi: 10.1190/1.1438450.
Aster, R. C., B. Borchers, and C. H. Thurber, 2012, Parameter estimation and inverse problems, 2nd ed.: Academic Press.
Bakulin, A., and R. Calvert, 2006, The virtual source method: Theory and case study: Geophysics, **71**, no. 4, SI139–SI150, doi: 10.1190/1.2216190.
Behura, J., 2007, Virtual Real Source: 77th Annual International Meeting, SEG, Expanded Abstracts, 2693–2697.
Behura, J., K. Wapenaar, and R. Snieder, 2012, Newton-Marchenko-Rose imaging: 82nd Annual International Meeting, SEG, Expanded Abstracts, 1–6.
Broggini, F., and R. Snieder, 2012, Connection of scattering principles: A visual and mathematical tour: European Journal of Physics, **33**, 593–613, doi: 10.1088/0143-0807/33/3/593.
Buland, A., and H. Omre, 2003, Bayesian wavelet estimation from seismic and well data: Geophysics, **68**, 2000–2009, doi: 10.1190/1.1635053.
Calvert, R., A. Bakulin, and T. Jones, 2004, Virtual sources, a new way to remove overburden problems: 66th International Annual Conference and Exhibition, EAGE, Extended Abstracts, P234.
Campillo, M., and A. Paul, 2003, Long-range correlations in the diffuse seismic coda: Science, **299**, 547–549, doi: 10.1126/science.1078551.
Curtis, A., P. Gerstoft, H. Sato, R. Snieder, and K. Wapenaar, 2006, Seismic interferometry — turning noise into signal: The Leading Edge, **25**, 1082–1092, doi: 10.1190/1.2349814.

Derode, A., E. Larose, M. Campillo, and M. Fink, 2003a, How to estimate the Green's function for a heterogeneous medium between two passive sensors? Application to acoustic waves: Applied Physics Letters, **83**, 3054–3056, doi: 10.1063/1.1617373.
Derode, A., E. Larose, M. Tanter, J. de Rosny, A. Tourin, M. Campillo, and M. Fink, 2003b, Recovering the Green's function from far-field correlations in an open scattering medium: Journal of the Acoustical Society of America, **113**, 2973–2976, doi: 10.1121/1.1570436.
Draganov, D., K. Wapenaar, and J. Thorbecke, 2006, Seismic interferometry: Reconstructing the earth's reflection response: Geophysics, **71**, no. 4, SI61–SI70, doi: 10.1190/1.2209947.
Dragoset, B., 2000, Introduction to airguns and air-gun arrays: The Leading Edge, **19**, 892–897, doi: 10.1190/1.1438741.
Gonzalez, R. C., R. E. Woods, and S. L. Eddins, 2003, Digital image processing using MATLAB: Prentice Hall.
Hargreaves, N. D., 1992, Air-gun signatures and the minimum-phase assumption: Geophysics, **57**, 263–271, doi: 10.1190/1.1443239.
Keys, R. G., and D. J. Foster, eds., 1998, Comparison of seismic inversion methods on a single real data set: SEG.
Komatitsch, D., and J. P. Vilotte, 1998, The spectral element method: An efficient tool to simulate the seismic response of 2D and 3D geological structures: Bulletin of the Seismological Society of America, **88**, 368–392.
Landrø, M., J. Langhammer, R. Sollie, L. Amundsen, and E. Berg, 1994, Source signature determination from mini streamer data: Geophysics, **59**, 1261–1269, doi: 10.1190/1.1443683.
Landrø, M., and R. Sollie, 1992, Source signature determination by inversion: Geophysics, **57**, 1633–1640, doi: 10.1190/1.1443230.
Lobkis, O., and R. Weaver, 2001, On the emergence of the Green's function in the correlations of a diffuse field: Journal of the Acoustical Society of America, **110**, 3011–3017, doi: 10.1121/1.1417528.
Oldenburg, D. W., S. Levy, and K. P. Whittall, 1981, Wavelet estimation and deconvolution: Geophysics, **46**, 1528–1542, doi: 10.1190/1.1441159.
Osen, A., B. G. Secrest, L. Amundsen, and A. Reitan, 1998, Wavelet estimation from marine pressure measurements: Geophysics, **63**, 2108–2119, doi: 10.1190/1.1444504.
Pratt, R. G., and R. M. Shipp, 1999, Seismic waveform inversion in the frequency domain, Part 2: Fault delineation in sediments using crosshole data: Geophysics, **64**, 902–914, doi: 10.1190/1.1444598.
Ravaut, C., S. Operto, L. Improta, J. Virieux, A. Herrero, and P. DellAversana, 2004, Multiscale imaging of complex structures from multifold wide-aperture seismic data by frequency-domain full-waveform tomography: Application to a thrust belt: Geophysical Journal International, **159**, 1032–1056, doi: 10.1111/j.1365-246X.2004.02442.x.
Robinson, E. A., and S. Treitel, 1980, Geophysical signal analysis: Prentice-Hall Inc.
Rose, J. H., 2002a, Time reversal, focusing and exact inverse scattering, 1st ed.: Springer-Verlag, 97–105.
Rose, J. H., 2002b, Single-sided autofocusing of sound in layered materials: Inverse Problems, **18**, 1923–1934, doi: 10.1088/0266-5611/18/6/329.
Schuster, G., J. Yu, J. Sheng, and J. Rickett, 2004, Interferometric/daylight seismic imaging: Geophysical Journal International, **157**, 838–852, doi: 10.1111/j.1365-246X.2004.02251.x.
Shapiro, N., M. Campillo, L. Stehly, and M. Ritzwoller, 2005, High-resolution surface-wave tomography from ambient seismic noise: Science, **307**, 1615–1618, doi: 10.1126/science.1108339.
Snieder, R., 2004, Extracting the Green's function from the correlation of coda waves: A derivation based on stationary phase: Physical Review E, **69**, 046610, doi: 10.1103/PhysRevE.69.046610.
Snieder, R., K. Wapenaar, and K. Larner, 2006, Spurious multiples in seismic interferometry of primaries: Geophysics, **71**, no. 4, SI111–SI124, doi: 10.1190/1.2211507.
Snieder, R., K. Wapenaar, and U. Wegler, 2007, Unified Green's function retrieval by cross-correlation; connection with energy principles: Physical Review E, **75**, 036103, doi: 10.1103/PhysRevE.75.036103.
Tenghamn, R., S. Vaage, and C. Borresen, 2007, A dual-sensor towed marine streamer: Its viable implementation and initial results: 77th Annual International Meeting, SEG, Expanded Abstracts, 989–993.
Verschuur, D., and A. Berkhout, 1997, Estimation of multiple scattering by iterative inversion, Part II: Practical aspects and examples: Geophysics, **62**, 1596–1611, doi: 10.1190/1.1444262.
Wapenaar, K., F. Broggini, E. Slob, and R. Snieder, 2013, Three-dimensional single-sided Marchenko inverse scattering, data-driven focusing, Green's function retrieval, and their mutual relations: Physical Review Letters, **110**, no. 8, 084301, doi: 10.1103/PhysRevLett.110.084301.
Wapenaar, K., and J. Fokkema, 2006, Green's function representations for seismic interferometry: Geophysics, **71**, no. 4, SI33–SI46, doi: 10.1190/1.2213955.
Wapenaar, K., J. Thorbecke, and D. Draganov, 2004, Relations between reflection and transmission responses of three-dimensional inhomogeneous media: Geophysical Journal International, **156**, 179–194, doi: 10.1111/j.1365-246X.2003.02152.x.

Weaver, R., and O. Lobkis, 2004, Diffuse fields in open systems and the emergence of the Green's function: Journal of the Acoustical Society of America, **116**, 2731–2734, doi: 10.1121/1.1810232.

Weglein, A. B., and B. G. Secrest, 1990, Wavelet estimation for a multidimensional acoustic or elastic earth: Geophysics, **55**, 902–913, doi: 10.1190/1.1442905.

Yilmaz, O., 2001, Seismic data processing, *in* Investigations in geophysics 2: SEG.

Ziolkowski, A., 1993, Determination of the signature of a dynamite source using source scaling, Part 1: Theory: Geophysics, **58**, 1174–1182, doi: 10.1190/1.1443501.